DOI: 10.1478/AAPP.1011A3

AAPP | Atti della Accademia Peloritana dei Pericolanti
Classe di Scienze Fisiche, Matematiche e Naturali
ISSN 1825-1242

Vol. 101, No. 1, A3 (2023)

SHEAR-FLOW-INDUCED DISTORTION OF THE DENSITY DISTRIBUTION AND TRANSITION FROM A STATIONARY TO AN INSTATIONARY NON-EQUILIBRIUM STATE OF A COLLOIDAL PARTICLE IN A TRAP

LEA FERNANDEZ [a], SIEGFRIED HESS [a*] AND SABINE H. L. KLAPP [a]

ABSTRACT. The motion of a colloidal particle in a liquid, confined within an optical trap and subjected to a shear flow, is modeled as an overdamped harmonic oscillator in n dimensions. The first n_{obs} components are associated with the observable variables, while the remaining $n_{int} = n - n_{obs}$ components are treated as "internal" or auxiliary variables intended to model complex fluid behavior. Coupling between the components drives the system into a non-equilibrium state. The Smoluchowski equation for the positional density distribution function is used to derive relaxation equations for the relevant averages. Specific results are presented for a plane Couette flow and for the case $n_{obs} = 2$ and $n_{int} = 1$. The shear-flow-induced effects on the observable averages and on the deformation and preferential orientation of the density distribution are analyzed and compared with numerical data from Brownian Dynamics simulations. A transition from a stationary to a transient state, corresponding to a delocalization of the particle or an escape from the trap, is found when the shear rate of the imposed stationary flow exceeds a critical value.

1. Introduction

Simple models may describe complex dynamic phenomena. This holds true for the overdamped harmonic oscillator, subjected to fluctuating forces, when applied to the motion of a colloidal particle in an optical trap (Franosch *et al.* 2011), in the presence of a shear-flow. The dynamics of the n components of the oscillator is formulated via Langevin equations involving deterministic forces linear in the components and fluctuating forces. Given the diagonal force coefficients (*i.e.* the spring constant), the friction coefficient and the temperature, the fluctuating forces are chosen such that the system is in equilibrium, when the components are mutually uncoupled. The non-diagonal coupling between the components drives the system into a non-equilibrium state. The first n_{obs} components are associated with the observable variables which can also be influenced by external fields, while the remaining $n_{int} = n - n_{obs}$ components are treated as "internal" or auxiliary variables, intended to model more complex fluid behavior. This concept was used previously to elucidate the non-Markovian behavior of the observed variables (Siegle *et al.* 2010) and

to compute time-correlation functions (Mitterwallner *et al.* 2020; Doerries *et al.* 2021). There, most of the results were for $n_{obs} = 1$ and $n_{int} = 1$ or $n_{int} = 2$.

Here we use Brownian dynamics (BD) simulations to obtain numerical solutions of the Langevin equations and we apply the Smoluchowski equation for the positional density distribution function to derive relaxation equations, also referred to as dynamical equations for the relevant averages which, in turn, determine the density distribution. Results are presented for the case $n_{obs} = 2$ and $n_{int} = 1$. The coupling between the two observed components is assumed to be given by the velocity gradients of a viscous flow, in particular by a shear flow corresponding to the plane Couette geometry. Despite the seeming simplicity of treating linear deterministic forces, just for the case $n = 3$, the coupling with the one additional auxiliary variable involves 4 additional coupling coefficients. This gives considerable "freedom" in modeling the dynamics but, at the same time, one has to make appropriate choices of parameters for the presentation of specific analytic and numerical results. Analytic solutions are available in full generality for the averages determining the density distribution in a stationary state. Here however, we focus the attention on the case of a plane Couette flow where the coupling with the internal variable is chosen such that it acts like a hidden variable, where no effect is noticed as long as the shear rate is not turned on. For non-zero shear rates not only a quantitative influence of the internal variable is observed, but also a surprising qualitative change when the shear rate exceeds a critical value: a transition from a stationary non-equilibrium state to a transient state occurs, even though the imposed shear flow is steady. This phenomenon corresponds to a delocalization of the colloidal particle, essentially to an escape from the trap although there is no potential threshold. We show that a source-sink type set-up allows to control the motion of the colloidal particle beyond the critical shear rate. Trajectories and contour plots of the probability density inferred form Brownian dynamics simulations elucidate the pre- and post-critical behavior.

When the concept of internal variables is applied for the macroscopic or mesoscopic treatment of complex media, thermodynamical considerations and mechanical stability arguments have to be taken into account (Restuccia and Kluitenberg 1988, 1990; Maugin and Muschik 1994; Francaviglia *et al.* 2004; Hess *et al.* 2008; Loos and Klapp 2020; Marteynec *et al.* 2020; Doerries *et al.* 2021). Without the coupling to an internal variable, the influence of a shear flow on the Brownian motion has been studied before, for diffusion (*e.g.*, see Foister and van de Ven 1980; Hess and Rainwater 1984). The probability distribution for a colloidal particle in a trap was presented by Bammert and Zimmermann (2010) and Holzer *et al.* (2010) . For a numerical study of diffusion under shear in an interactive system see Vezirov and Klapp (2013).

This article proceeds as follows. First, in Sec. **2**, the model is formulated for the general n-dimensional case via Langevin equations. The tools for the study of solutions and their consequences for physical phenomena, *viz.* Brownian dynamics simulations and the Smoluchowski equation, are presented in Sec. **2.2** and Sec. **2.3**. Following basic considerations, thermal equilibrium and deviations from it, as well as entropy production rate are discussed in Sec. **2.3.2**. The dynamics of averages of quantities depending on the position variables follows from the Smoluchowski equation, Sec. **2.3.3**. The relaxation equations for averages linear and bilinear in the position variables, called linear and bilinear averages, are discussed in Sec. **2.3.4** and Sec. **2.3.5**. As pointed out in Sec. **2.3.6**, the bilinear

averages determine the positional probability density which is Gaussian, also for many non-equilibrium situations. Section **3** is devoted to the case of a two-dimensional oscillator coupled with one internal variable. The specific model is introduced and details of the couplings are discussed in Sec. **3.1**. Trajectories and probability densities, as computed by BD, are displayed in Sec. **3.2** and in Sec. **3.3.2**. Section **3.4.1** is devoted to a comparison of analytic solutions for averages of interest, in the pre-critical stationary state, with the corresponding results from BD simulations. Special attention is paid to the observed singularity at the critical shear rate as well as to the numerical solutions for the post-critical source-sink flow arrangement where a flux or transit rate is observed. A scaling relation for the latter quantity and a further indicator for the occurrence of the critical shear rate are presented in Sec. **3.4.3** and Sec. A.**2**. The apparent continuity, across the singularity of the analytic solutions, for the flow alignment angle and the eccentricity is tested in Sec. A.**3**.

In the concluding remarks, it is conjectured that the present analysis for a colloidal particle in a trap can be adapted to the study of the deformation and orientation of polymer molecules in a dilute solution, subjected to a shear flow.

2. The model and the methods

2.1. Overdamped n-dimensional harmonic oscillator.

2.1.1. *Forces and coupling coefficients.* Let $x \in V \subseteq \mathbb{R}^n$, $n = 1,2,\ldots$ be the position vector of a harmonic oscillator with the components $x_i = x_i(t)$, $i = 1,..,n$, $t \in [0,\infty)$, t being the time. For most applications, the domain V is equal to $\mathbb{R}^n$. The components of the systematic force $F \in \mathbb{R}^n$ are given by

$$F_i = -a^{(i)} x_i + \tilde{F}_i\,, \quad \tilde{F}_i = M_{ij} x_j\,, \quad \text{with } M_{ij} = 0\,, \text{for } i = j\,. \tag{1}$$

The summation convention is used for subscripts, but not for superscripts. Thus $M_{ij}x_j$ stands for $\Sigma_{j=1}^n M_{ij}x_j$, however there is no summation over i in the expression $a^{(i)}x_i$. The $a^{(i)} > 0$ are the diagonal force coefficients of the oscillator, corresponding to spring constants . For $\tilde{F} = (\tilde{F}_1, \cdots, \tilde{F}_n) = 0$, the components are mutually independent. The coupling between these components is caused by $\tilde{F} \neq 0$ with the purely non-diagonal matrix $M \in \mathbb{R}^n \times \mathbb{R}^n$. In general, the matrix M is not symmetric: $M_{ij} \neq M_{ij}$.

2.1.2. *Langevin equations.* Let the damping of the motion of the oscillator be determined by the friction coefficient γ. Here the friction is characterized by a symmetric second rank tensor with the eigenvalues $\gamma^{(i)} > 0$. It is assumed that a coordinate system exists where both the force coefficients a and the friction coefficients γ are represented by diagonal matrices. Fluctuating forces $\zeta \in \mathbb{R}^n$ ensure that the oscillator does not come to rest at $x = 0$. The overdamped dynamics considered here corresponds to the case where the product of a characteristic oscillation frequency $\omega_{osc} = \sqrt{a_{ref}/m}$ with the damping time $t_{dmp} = m/\gamma_{ref}$ is less than 1, where m is the relevant mass, a_{ref} and γ_{ref} are representative values of the diagonal force constants $a^{(i)}$ and of the friction coefficients $\gamma^{(i)}$. Assuming "white noise" type fluctuating forces, the time change $\dot{x} = dx/dt$ of the components is governed by the Langevin equations (Langevin 1908; Kubo 1966; Risken 1984)

$$\dot{x}_i = (\gamma^{(i)})^{-1}(F_i + \zeta_i)\,, \quad \zeta_i = (2k_B T\,\gamma^{(i)})^{1/2}\,\xi_i\,, \text{ with } \langle \xi_i(t)\,\xi_j(t')\rangle = \delta_{ij}\,\delta(t-t')\,. \tag{2}$$

Here $\langle \ldots \rangle$ indicates an average, T is the temperature and k_B stands for the Boltzmann constant. For $\tilde{F} = 0$ and in thermal equilibrium, the long time limit of this resulting mean square displacement of the component x_i and the equal-time correlations $\langle x_i x_j \rangle$ are given by

$$\langle (x_i(t) - x_i(0))^2 \rangle = \langle x_i^2 \rangle_{eq} \equiv \frac{k_B T}{a^{(i)}}, \quad \langle x_i x_j \rangle = \langle x_i x_j \rangle_{eq} \equiv 0 \text{ for } i \neq j. \tag{3}$$

In contrast, when $M \neq 0$ and thus $\tilde{F} \neq 0$, the averages of the bilinear quantities x_i^2 and $x_i x_j$ differ from their equilibrium values, as shown in the following. The effect of $M \neq 0$ on these averages is analyzed and presented for some specific choices of the coupling coefficients.

2.1.3. *Dimensionless variables.* Dimensionless friction and force coefficients are introduced by dividing γ as well as a and M by conveniently chosen reference values γ_{ref} and a_{ref}, similarly the temperature is expressed in terms of a reference temperature T_{ref}. For the overdamped harmonic oscillator, appropriate reference variables t_{ref} and x_{ref} for the time and length are defined by

$$t_{ref} = \gamma_{ref}/a_{ref}, \quad x_{ref}^2 = k_B T_{ref}/a_{ref}. \tag{4}$$

Observing that $\delta(t) = (t_{ref})^{-1}\, \delta(t/t_{ref})$, expressing ξ in units of $(t_{ref})^{-1/2}$ and using the same names for the dimensionless variables as for the original ones, the Langevin equations just read as (2), but with $k_B = 1$. Furthermore, one may absorb the dimensionless friction coefficients $\gamma^{(i)}$ into the dimensionless force coefficients $a^{(i)}, M_{ij}$ and introduce "temperature" coefficients $T^{(i)}$ according to

$$(a^{(i)})^* = (\gamma^{(i)})^{-1} a^{(i)}, \quad (M_{ij})^* = (\gamma^{(i)})^{-1} M_{ij}, \quad T^{(i)} = (\gamma^{(i)})^{-1} T. \tag{5}$$

In some applications different temperature variables are studied and even needed in (2) and (3) instead of the common temperature T (see Filliger and Reimann 2007; Cerasoli *et al.* 2018; Loos and Klapp 2020). Then the temperature variables $T^{(i)}$ are different even when all $\gamma^{(i)}$ are equal to each other. Renaming $a^*, M^* \to a, M$, the rescaled Langevin equations read

$$\dot{x}_i = -a^{(i)} x_i + M_{ij} x_j + \zeta_i, \quad \zeta_i = (2T^{(i)})^{1/2}\, \xi_i, \text{ with } \langle \xi_i(t)\, \xi_j(t') \rangle = \delta_{ij}\, \delta(t - t'). \tag{6}$$

Here all variables and model coefficients are dimensionless, as anyway required in the numerical calculations of the Brownian dynamics simulations. In the applications to be presented later, for simplicity, all friction coefficients are assumed to be equal and all $T^{(i)}$ correspond to one temperature variable T. Notice, the scaling used here for the overdamped dynamics does not involve the mass m of the colloidal particle.

2.2. Brownian Dynamics. The numerical solution of the Langevin equations, with white noise random forces, is referred to as Brownian dynamics. The continuous time variable t is discretized into time steps of equal length δt. Before the dynamics calculations are started, lists of Gaussian random numbers needed for the total number of time steps $N_{run} = t_{run}/\delta t$ within a simulation run of time length t_{run} are generated, centered, normalized and the orthogonality of the random number used for the different components, is tested. Then sequences of positions $x_i(t_n)$, $n = 1, .., N_{run}$ at the time steps t_n are computed with an Euler integration scheme.

Both the simple explicit Euler method as well as a modified Euler method were tested. The latter one, which is akin to the Störmer-Verlet method (Verlet 1967), involves two half-step midpoint Euler steps where the forces are computed just once per step, but the length of the time step is twice that of the simple Euler method. On the other hand, for a continuous force, the integration error is of order δt^3, times the second spatial derivative of the deterministic force, whereas for the simple Euler method, it is of order δt^2, times the first spatial derivative of the deterministic force. See the appendix for details. The results to be presented here were computed with the modified Euler method.

Typical numbers for N_{run} are 10^3 to 10^6. Results of the simulations can be visualized as trajectories or in density plots. Averages of physical quantities of interest are inferred from the positions x_i according to the rules of Statistical Physics. Much as with Molecular Dynamics (MD) (Verlet 1967; Allen and Tildesley 2017), Non-Equilibrium Molecular Dynamics (NEMD) (Evans *et al.* 1984; Hoover 1986; Hess *et al.* 1996; Evans and Morriss 2008) and Stokesian Dynamics (Brady and Bossis 1988; Gerloff *et al.* 2020) simulations, this can be viewed as using measuring devices to obtain "computer experimental data". Shorter time steps are appropriate for generating trajectories, density plots and correlation functions, longer time steps are applied for the computation of long time averages in stationary states.

Prior to the results presented below, test calculations were performed, for ordinary diffusion and, in particular, for the particle in the harmonic trap. The comparison of computed static equilibrium properties and time correlation functions with the corresponding analytic expressions confirmed the reliability of the Brownian dynamics simulations. The numerical data and graphs were computed with Mathematica 13, also test calculations and cross checks were performed with the older version Mathematica 5. For a particular choice of the model parameters, BD provides trajectories of the particle and successive positions which essentially represent the positional probability density, see Figs. 2 and 3. Furthermore, averages $\langle \psi \rangle$ of functions $\psi = \psi(x(t))$ are computed as time-averages. Most important are averages of quantities linear and bilinear in x, *i.e.* the linear averages $\langle x_i \rangle$ and the bilinear averages $\langle x_i x_j \rangle$. Examples are discussed in Sec. **3.4**. Of particular interest is also the kurtosis $\langle x_i^4 \rangle - 3\langle x_i^2 \rangle^2$, assuming $\langle x_i \rangle = 0$, which vanishes for a Gaussian distribution. The relative kurtosis

$$\kappa^{(i)} = \frac{\langle x_i^4 \rangle}{3\langle x_i^2 \rangle^2} - 1\,, \tag{7}$$

is a measure for the deviation from Gaussian behavior. Time-correlation functions like the positional auto-correlation function $C_{ii}(\tau) = \langle x_i(t+\tau)x_i(t) \rangle$, depending just on the time difference τ and not on t, for fluctuations in equilibrium or stationary non-equilibrium states, can and have been computed via BD for the model systems considered, but are outside the scope of this article.

2.3. Smoluchowski Equation.

2.3.1. *Basic considerations.* The Smoluchowski equation (SE) is a partial differential equation (first order in time, second order in position) for a "density" function which tells us the probability to find a particle in a n-dimensional domain, denoted by V, at the Cartesian

coordinates $x = (x_1, \cdots, x_n)$ at a time t from a time interval I. This multidimensional probability density is here called $\rho(x,t)$.

Let $\rho = \rho(x,t) : \{V,I\} \to \mathbb{R}$, with domain $V \subseteq \mathbb{R}^n$ and the time interval $I \subseteq \mathbb{R}$. This means that ρ is a scalar function with arguments $x = (x_1, \cdots, x_n) \in V \subseteq \mathbb{R}^n$, and time $t \in I$. We require that ρ be twice differentiable and once integrable. The interpretation of x will vary depending on the physical problems we are looking at in different sections, it can contain what we will later call the components of the position vector of our colloidal particle as well as what we consider as auxiliary variables. We interpret ρ as a probability density with $\int_V \rho(x,t)dx = 1$ for all $t \in I$, dx being multidimentional. The continuity equation

$$\partial_t \rho(x,t) + \partial_x j(x,t) = 0 \tag{8}$$

guarantees that the normalisation stays constant for all times. In the case of diffusion in the presence of a force, which is a vector $F = (F_1, \cdots, F_n) = F(x,t) : \{V,I\} \to \mathbb{R}^n$ the current density is (de Groot and Mazur 1962)

$$j = j(x,t) = \gamma^{-1}(F(x,t)\rho(x,t) - k_B T \partial_x \rho(x,t)) . \tag{9}$$

Here γ is the friction coefficient, $\mu = \gamma^{-1}$ is the mobility, $D = k_B T \gamma^{-1} = k_B T \mu$ is the diffusion coefficient and T is the temperature, k_B is the Boltzmann constant. In general, the material coefficients γ, μ and D are second rank tensors. As before, we shall assume that these coefficients are represented by diagonal matrices with positive principal values, just as the force coefficient a. It is assumed that these matrices are diagonalized in the same rectangular coordinate system and furthermore, that all material coefficients are independent of t and x. Inserting equation (9) into the continuity equation we get the Smoluchowski equation

$$\partial_t \rho + \partial_x \gamma^{-1}(F\rho - k_B T \partial_x \rho) = 0 . \tag{10}$$

In component notation and with $\partial_t \equiv \frac{\partial}{\partial t}$, $\partial_i \equiv \frac{\partial}{\partial x_i}$ the Smoluchowski equation reads

$$\partial_t \rho + \partial_i (\gamma^{(i)})^{-1}(F_i \rho - k_B T \, \partial_i \rho) = 0 . \tag{11}$$

It is understood that the summation convention applies to subscripts. Next, the rescaled version of the Smoluchowski equation is stated which corresponds to the Langevin equations (6) where the friction coefficients $\gamma^{(i)}$ are absorbed into the force coefficients and the parameters $T^{(i)}$. In component notation, it reads

$$\partial_t \rho + \partial_i \left((-a^{(i)} x_i + M_{ij} x_j) \rho - T^{(i)} \partial_i \rho \right) = 0 . \tag{12}$$

It is recalled that the summation convention applies to the subscripts, but not to the superscripts which indicate principal values. This means that *e.g.* $\partial_i (a^{(i)} x_i \rho)$ stands for $\Sigma_{i=1}^n \partial_i (a^{(i)} x_i \rho)$.

The theoretical approach based on the Smoluchowski equation (Smoluchowski 1916) is practically equivalent to the treatment with the Langevin equation for the overdamped case. The same applies to the numerical computations for the variables x_i, $i = 1, \cdots, n$, which is referred to as Brownian Dynamics. The Smoluchowski equation (11) is also called Fokker-Planck equation (cf. Risken 1984). Brief remarks on the equations introduced by Fokker and by Planck and the connection with the Smoluchowski equation, as well as

on generalizations of these kinetic equations are in order. Starting from Planck's version (Planck 1917) of the Fokker-Planck equation (FPE) for the velocity distribution function, with an external force taken into account as by Kramers (1940), an equation for the flux density j can be derived which contains an additional term involving $\partial_t j$. The overdamped case applies to physical situations where the "inertia term" $\partial_t j$ can be neglected, as tacitly assumed in (9). A variant of the kinetic equation (11) is the Kirkwood-Smoluchowski equation (Kirkwood 1946) where ρ stands for the pair-correlation function $g = g(x)$ of a dense fluid composed of spherical, non-rotating particles. The original Fokker version (Fokker 1914) of the FPE deals with the orientational distribution function depending on a vector specifying the direction of a non-spherical particle whose rotational motion is overdamped. The application to flow birefringence in dispersions of rod-like particles was presented by Peterlin and Stuart (1943), generalizations to flow alignment phenomena in the isotropic and nematic phases of liquid crystals were introduced by Hess (1976) and Doi (1980) (see also Doi and Edwards 1986; Forest *et al.* 2004; Kröger 2004; Emmrich *et al.* 2018). Futhermore, FPE's for systems with time delay, corresponding to infinitely many auxiliary variables with non-reciprocal coupling were introduced and discussed by Loos and Klapp (2019, 2020).

2.3.2. *Thermal equilibrium, deviation from equilibrium and entropy production rate.* In the presence of an external potential $\Phi = \Phi(x) \in \mathbb{R}$ and in thermal equilibrium with the temperature T, the probability density ρ is equal to the equilibrium density $\rho_{eq} \sim \exp(-\beta\,\Phi)$ and we have

$$\partial_x \rho_{eq} = -\beta\,\rho_{eq}\partial_x\Phi\,, \quad \beta = 1/(k_B T)\,. \tag{13}$$

For $F = -\partial_x\Phi$ the flux density j vanishes in equilibrium and consequently $\partial_t\rho_{eq} = 0$, as expected. When F is not equal to $-\partial_x\Phi$, in particular for

$$F = -\partial_x\Phi + \tilde{F}\,, \quad \tilde{F} \neq 0\,, \tag{14}$$

the Smoluchowski equation not only describes the approach to thermal equilibrium, but also stationary non-quilibrium states can occur, when the "extra"-force $\tilde{F}$ does not depend on the time t. Notice that $\tilde{F}$ (which correspond to the $\tilde{F}$ of equation (1)) in general is a sum of a contributions which can and another one which cannot be derived from a potential function.

The probability density ρ, in general, deviates from the equilibrium density ρ_{eq}. The quantity $\varphi = \varphi(t,x)$, defined by $\rho = \rho_{eq}(1+\varphi)$ is a measure for this deviation. In fluids composed of many particles, this deviation is small such that it suffices to linearize the relevant kinetic equations in φ. This is not meaningful for the dynamics of a single particle which has to cary the "load" of the deviation from equilibrium alone. Large deviations from equilibrium are encountered in this case. So it is appropriate to write $\rho = \rho_{eq}(\rho/\rho_{eq})$ and not to expand with respect to powers of $(\rho/\rho_{eq}) - 1$. The flux density j given by (9) is equivalent to

$$j = (\gamma)^{-1}\left(\rho\,(F + \partial_x\Phi) - k_B T\,\rho_{eq}\partial_x(\rho/\rho_{eq})\right) = (\gamma)^{-1}\left(\rho\tilde{F} - k_B T\,\rho_{eq}\partial_x(\rho/\rho_{eq})\right)\,. \tag{15}$$

Due to $\rho_{eq}\partial_x(\rho/\rho_{eq}) = \rho\,\partial_x\ln(\rho/\rho_{eq})$, the Smoluchowski equation (10) is equivalent to

$$\partial_t\rho = \partial_x(\gamma)^{-1}\left(k_B T\,\rho\,\partial_x\ln(\rho/\rho_{eq}) - \rho\,\tilde{F}\right)\,. \tag{16}$$

This expression is used for the proof of the irreversibility of the Smoluchowski equation. Subject to the assumption that the surface contributions vanish, the entropy production rate $\dot{\Theta}$ is determined by

$$T\,\dot{\Theta} = \int dx \rho \left(k_B T \frac{\partial}{\partial x} \ln(\rho/\rho_{eq}) - \tilde{F} \right) (\gamma)^{-1} \left(k_B T \frac{\partial}{\partial x} \ln(\rho/\rho_{eq}) - \tilde{F} \right). \quad (17)$$

Here $T\dot{\Theta}$ is essentially the heat of friction per unit time, generated by the pertaining irreversible processes. Obviously we have $\dot{\Theta} \geq 0$, provided that the principal values of γ are positive. The result (17) is not restricted to the special potential and the forces used in the following applications. For $\tilde{F} = 0$, the expression (17) reduces to the corresponding relation derived by Doi and Edwards (1986). The expression (17) is equivalent to

$$T\,\dot{\Theta} = \int dx \, (j(x,t)\,\gamma\, j(x,t))\,\rho^{-1}, \quad (18)$$

which was derived for the ensemble-averaged entropy production rate by Seifert (2005, 2012) using concepts from stochastic thermodynamics. In component notation and with the "velocity" $v(x,t) = \gamma\, j(x,t)\,\rho^{-1}$, the expression (18) reads

$$T\,\dot{\Theta} = \int dx \, (j(x,t)_i\, v(x,t)_i), \quad v_i = F_i - k_B T\, \partial_i ln\rho\,. \quad (19)$$

In a stationary state where $\partial_i j_i = 0$ holds true, for F given by (1) with $a^{(i)} = a$ and when surface contributions play no role, the expression for the entropy production reduces to

$$T\,\dot{\Theta} = M^a_{ki} M_{kj} < x_i x_j >, \quad M^a_{ki} = (1/2)(M_{ki} - M_{ik})\,. \quad (20)$$

Here M^a is the antisymmetric part of the coupling matrix M. Thus, in accord with Loos and Klapp (2020), one has $\dot{\Theta} = 0$ for a symmetric coupling where $M_{ki} = M_{ik}$ applies. A detailed discussion of the entropy production and heat exchange for the model system treated here is outside the scope of this article.

2.3.3. *Dynamics of averages.* The average $\langle\Psi\rangle$ of $\Psi = \Psi(x)$ is defined via the integration over the volume $V \subseteq \mathbb{R}^n$:

$$\langle\Psi\rangle = \int_V \Psi(x)\rho(x)\,dx, \quad \int_V \rho(x)\,dx = 1\,. \quad (21)$$

The average evaluated with the equilibrium density ρ_{eq} is denoted by $\langle\ldots\rangle_{eq}$, thus

$$\langle\Psi\rangle_{eq} = \int_V \Psi(x)\rho_{eq}(x)\,dx, \quad \int_V \rho_{eq}(x)\,dx = 1\,. \quad (22)$$

Multiplication of (10) with $\Psi(x)$ and integration by parts lead to

$$\frac{d}{dt}\langle\Psi\rangle - \left[\langle (\frac{\partial}{\partial x}\Psi)(\gamma)^{-1} F\rangle - k_B T \int_V (\frac{\partial}{\partial x}\Psi)\,(\gamma)^{-1} (\frac{\partial}{\partial x}\rho) dx \right] = 0\,. \quad (23)$$

The further integration by parts of the second term in the bracket $[\ldots]$ yields

$$\frac{d}{dt}\langle\Psi\rangle - \left[\langle(\frac{\partial}{\partial x}\Psi)(\gamma)^{-1}F\rangle + k_BT\,\langle\frac{\partial}{\partial x}(\gamma)^{-1}\frac{\partial}{\partial x}\Psi\rangle\right] = 0\,. \tag{24}$$

These calculations are exact under the assumption that there are no surface contributions. In the following, rescaled variables are used, thus $t, x, F, T, ..$ are expressed in reduced units, as in Sec. **2.1.3**. For the scaled variables the same "names" are used as for the original variables. The resulting equations correspond to the equations stated above, now with $\gamma = 1$ and $k_B = 1$. The equation (24) for the dynamics of the averages then reads

$$\frac{d}{dt}\langle\Psi\rangle - \langle(\frac{\partial}{\partial x_i}\Psi)F_i\rangle - \Sigma_i T^{(i)}\langle\frac{\partial^2}{\partial x_i^2}\Psi)\rangle = 0\,. \tag{25}$$

Notice: when we used integration by parts, it was assumed that surface contributions vanish.

2.3.4. *Linear averages.* The averages of quantities linear and bilinear in the components of x are referred to as "linear" and "bilinear averages", they are also called first and second moments of the probability distribution.

For $\Psi = x_i$, equation (25) leads to the relaxation equations $\frac{d}{dt}\langle x_i\rangle - \langle F_i\rangle = 0$, or, with F_i determined by (1),

$$\frac{d}{dt}\langle x_i\rangle + a^{(i)}\,\langle x_i\rangle - M_{ij}\,\langle x_j\rangle = 0\,. \tag{26}$$

Here the diffusion term of the SE, involving the second spatial derivative, gives no contribution. The linear averages $\langle x_i\rangle$ decay to 0, as one can show by performing a stability analysis, provided that the determinant of the matrix

$$K = \mathsf{a} - M\,, \quad \mathsf{a} = diag(a^{(i)}\,, i = 1, .., n) \tag{27}$$

is positive definite. In general, K is not symmetric, just as M.

2.3.5. *Bilinear averages.* For $\Psi = x_i x_j$, equation (25) leads to the relaxation equations

$$\frac{d}{dt}\langle x_i x_j\rangle - \langle F_i x_j\rangle - \langle F_j x_i\rangle - 2T^{(i)}\,\delta_{ij} = 0\,. \tag{28}$$

In the following, we assume $T^{(i)} = T$, for all i, for simplicity. With F_i determined by (1) and using scaled variables, we have

$$\frac{d}{dt}\langle x_i x_j\rangle + (a^{(i)} + a^{(j)})\,\langle x_i x_j\rangle - M_{ik}\,\langle x_k x_j\rangle - M_{jk}\,\langle x_k x_i\rangle = 2\,T\,\delta_{ij}\,. \tag{29}$$

which is exact provided there are no surface contributions. Here the diffusion term of the SE, involving the second spatial derivative, gives contributions only in the equations for the quadratic averages $\langle x_i^2\rangle$. The bilinear averages scale with T, since (29) reduces to a homogeneous system of differential equations for $T = 0$.

2.3.6. *Gaussian probability distribution.* The bilinear averages $\langle x_i x_J \rangle$ determine the probability density when it is of Gaussian type. For deterministic forces linear in x and white noise, as considered here, this is indeed the case for the stationary solution of the Smoluchowski equation (see Risken 1984, Sec. 6.5). In the BD simulations this has to be tested. We found that the relative kurtosis $\langle x^4 \rangle (3\langle x^2 \rangle^2)^{-1} - 1$ is practically zero, even in all stationary non-equilibrium situations. Thus the numerical results are in accord with the Gaussian property of the probability distribution.

In the following, we express ρ, for the n dimensional case, in terms of the Gaussian function:

$$\rho \sim \exp\left[-\frac{1}{2}\frac{n}{R^2} A_{ij}^{-1} x_i x_j\right], \quad R^2 = \langle x_k x_k \rangle, \quad \frac{R^2}{n} A_{ij} = \langle x_i x_j \rangle. \tag{30}$$

For later applications, we decompose A_{ij} into its isotropic part δ_{ij} and its anisotropic (deviatoric) part Q_{ij} according to

$$A_{ij} = \delta_{ij} + \frac{n}{R^2} Q_{ij}, \quad Q_{ij} = \langle x_i x_j \rangle - \frac{R^2}{n} \delta_{ij}. \tag{31}$$

By definition, the matrices A and Q are symmetric. The "radius" R is a measure for the "size" of the density "cloud". Its "shape" and "orientation" are determined by the symmetric traceless tensor Q_{ij}, which has the symmetry of the "quadrupole moment tensor". For $Q_{ij} = 0$ the probability density is "isotropic", or "spherical symmetric". This means it does not possess any preferential direction. Thus $Q_{ij} \neq 0$ characterizes the "anisotropy" or the "deviation from isotropy". Examples are presented in Sec. **3.2** and Sec. **3.4** .

3. Two-dimensional oscillator coupled with one internal variable

3.1. The specific model.

3.1.1. *Preliminary remarks.* Now we have a more detailed view on variables, parameters and the formulation of relaxation equations as well as on physical interpretations. The case at hand corresponds to a three dimensional oscillator which we treat as an isotropic two-dimensional oscillator, two physical degrees of freedom, coupled to one internal variable. The two-dimensional oscillator represents a colloidal particle in an optical trap. The two coupling coefficients between its components are interpreted as being caused by a volume conserving shear flow, in particular of plane Couette or squeeze flow type. Special attention shall be devoted to the influence of a shear flow on the shape and orientation of trajectories and on the particle cloud representing the probability distribution. To emphasize the effect of the coupling with the third component x_3, involving four additional coupling coefficients, first results shall be shown for the case where the coupling with the auxiliary variable x_3 is turned off.

We consider the vector $x \in \mathbb{R}^3$ with components x_i, $i = 1,2,3$. In the following, the variables x_1 and x_2 are also denoted by x and y, when no danger of confusion exists. As before, the force is given by $F_i = -a^{(i)} x_i + M_{ij} x_j$ with $M_{ij} = 0$ for $i = j$ and, in general, $M_{ij} \neq M_{ji}$. The isotropic two-dimensional oscillator corresponds to $a^{(1)} = a^{(2)} = a$. Next we specify the coupling coefficients M_{12} and M_{21}.

3.1.2. *Flow geometry.* Let the force which couples the components x and y be caused by a divergence-free flow field v, with the components $v_x = v_x(x,y), v_y = v_y(x,y)$. The velocity gradient shall be constant. The coefficients M_{12} and M_{21} are given by

$$M_{12} = \frac{\partial v_x}{\partial y}\,, \quad M_{21} = \frac{\partial v_y}{\partial x}\,. \tag{32}$$

In the following, the main attention is devoted to the *plane Couette flow* as it occurs in a fluid confined by two flat plates, moving in opposite directions. Let the velocity be in x-direction, its gradient in y-direction. The constant *shear rate* is denoted by $\Gamma = \frac{\partial v_x}{\partial y}$, thus

$$M_{12} = \Gamma\,, \quad M_{21} = 0\,. \tag{33}$$

Clearly, here we encounter $M_{12} \neq M_{21}$. The symmetric case $M_{12} = M_{21}$ pertains to a planar *squeeze flow*, as realized in a *four-roller set up*, with the constant *deformation rate* or *extension rate* $\varepsilon = \frac{\partial v_x}{\partial y} = \frac{\partial v_y}{\partial x}$. Then we have

$$M_{12} = \varepsilon\,, \quad M_{21} = \varepsilon\,. \tag{34}$$

This type of flow is also called planar *extensional flow* or *biaxial extensional flow*. A solid-like *rotational flow* with angular velocity Ω_3 (rotation about the x_3-axis) corresponds to the antisymmetric coupling

$$M_{12} = \Omega_3\,, \quad M_{21} = -\Omega_3\,. \tag{35}$$

For a schematic sketch of the coupling schemes see the top row of Fig. 1. In general, linear combinations thereof are possible. Notice that the plane Couette flow with shear rate Γ is essentially a linear superposition of a planar extensional flow with $\varepsilon = \Gamma/2$ and a rotational flow with $\Omega_3 = -\Gamma/2$.

As suggested by a referee, a remark is added on the "Brownian Gyrator" (see Filliger and Reimann 2007; Cerasoli *et al.* 2018). The term gyrator refers to the torque or curl found in these studies. Their model is a two-dimensional, overdamped anisotropic harmonic oscillator, corresponding to a symmetric, spring-like coupling $M_{12} = M_{21}$, in our notation, and to $a^{(1)} \neq a^{(2)}$, for the diagonal force coefficients in the paper by Filliger and Reimann (2007). Cerasoli *et al.* (2018) takes into account an additional constant force. It should be stressed that different temperatures $T^{(1)} \neq T^{(2)}$ are essential for the interesting results obtained by Filliger and Reimann (2007) and Cerasoli *et al.* (2018).

3.1.3. *Remarks on stationary solutions of the relaxation equations.* A necessary condition for the existence of a stable stationary solution of the linear averages, see Sec. **2.3.4**, is

$$D_3 \equiv \det(K) = \det(\mathsf{a} - M) > 0\,, \tag{36}$$

where the determinant is now given by

$$D_3 = a^{(1)}a^{(2)}a^{(3)} - a^{(1)}M_{23}M_{32} - a^{(2)}M_{31}M_{13} - a^{(3)}M_{12}M_{21} - M_{12}M_{23}M_{31} - M_{21}M_{13}M_{32}\,. \tag{37}$$

It is understood that all $a^{(i)} > 0$. In the case of the two-dimensional overdamped harmonic oscillator, which is not coupled to x_3, the corresponding condition is

$$(a^{(1)}a^{(2)} - M_{12}M_{21})\,a^{(3)} > 0\,. \tag{38}$$

For plane Couette flow where $M_{12} = \Gamma$ and $M_{21} = 0$, this implies that stable stationary solutions exist for all values of the imposed shear rate Γ. The determinant is also positive for a rotational flow with the angular velocity Ω_3 where one has $M_{12} = -M_{21} = \Omega_3$. For the plane squeeze flow, on the other hand, where $M_{12} = M_{21} = \varepsilon$, the deformation rate ε must obey $\varepsilon < a^{(1)}a^{(2)}$. The coupling of the two-dimensional oscillator with the auxiliary variable x_3, involving four additional coefficients, affects these stability conditions. Out of the four-parameter space, some representative examples of special interest, shall be considered in the following.

The stationary solutions of the relaxation equations (29) for the six variables $\langle x_i^2\rangle$ and $\langle x_i x_j\rangle$, $i \neq j$, can be obtained from the stationary version ($\partial_t\langle x_i x_i\rangle = 0$) of the relaxation equations (29), now for $i, j = 1,2,3$. These are linear equations where only the diagonal quantities contain an inhomogeneity, proportional to T. Elimination or rather insertion of $\langle x_i^2\rangle$ into the three equations for $\langle x_i x_j\rangle$, $i \neq j$ yields three coupled equations which can be solved conveniently. The resulting expressions, computed analytically with the support of Mathematica, are proportional to T and, in general, highly nonlinear functions of the 9 parameters $a^{(i)}, M_{ij}$. More specifically, these expressions can be written as

$$\langle x_i^2\rangle = H^{(ii)}/D_6\,, \quad \langle x_i x_j\rangle = H^{(ij)}/D_6,\, i \neq j\,, \tag{39}$$

where the $H^{(..)}$ and the determinant D_6 are polynomials of fifth and sixth degree in the coefficients $a^{(i)}, M_{ij}$. We refrain from presenting the analytic results in full generality. However, plots of these analytic expressions for various sets of the coefficients are useful for a survey of different scenarios. The analytic expressions are simpler for special values of the coefficients, but even for $T = a^{(1)} = a^{(2)} = a^{(3)} = 1$ and for the Couette flow, where one puts $M_{12} = \Gamma$ and $M_{21} = 0$, still an educated choice has to be made for the 4 remaining coupling coefficients M_{23}, M_{32} and M_{31}, M_{13}. Later we impose the requirement that $\langle xy\rangle = 0$ for $\Gamma = 0$, just as in equilibrium, for the choice of a specific coupling scheme whose consequences are analyzed in more detail.

3.1.4. *Representative coupling schemes.* Now some typical cases for M_{23}, M_{32} and M_{31}, M_{13} are discussed and then we present the specific choice made for the following studies. First consider two special cases where two of the four coupling coefficients are zero. These are

(i) *pseudo-external coupling*, where the components x_1 and x_2 are influenced by x_3 but do not act back on x_3. Denoting the two parameters by π_1 and π_2, we write

$$M_{13} = \pi_1\,, \quad M_{23} = \pi_2\,, \quad M_{31} = M_{32} = 0\,. \tag{40}$$

(ii) *string-like coupling*, where in analogy to the Couette coupling in the x_1, x_2-plane, x_3 is influenced by x_1 and it acts back on x_2 only. Denoting here the parameters by Γ_1 and Γ_2, we have

$$M_{23} = \Gamma_1\,, \quad M_{31} = \Gamma_2\,, \quad M_{32} = M_{13} = 0\,. \tag{41}$$

In both cases (i) and (ii), the coupling coefficients are neither symmetric nor antisymmetric. This is different for the next coupling schemes, which involve 4 nonzero coefficients.

(iii) *spring-like symmetric coupling*, where we denote the coefficients by ε_1 and ε_2, in analogy to the squeeze flow coefficient. Here we have

$$M_{23} = M_{32} = \varepsilon_1 \,, \quad M_{31} = M_{13} = \varepsilon_2 \,. \tag{42}$$

(iv) *rotation-like antisymmetric coupling*, with the angular velocities Ω_1 and Ω_2 defined by

$$M_{23} = \Omega_1 = -M_{32} \,, \quad M_{31} = \Omega_2 = -M_{13} \,. \tag{43}$$

This setting is also referred to as *bi-rotational coupling*. For $\Gamma = 0$, and $a^{(1)} = a^{(2)} = a$, the stationary solutions, with $x_1 = x \,, x_2 = y$, yield

$$\langle xy \rangle = \frac{(a^{(3)} - a)\Omega_1 \, \Omega_2}{a(a + a^{(3)})(aa^{(3)} + \Omega_1^2 + \Omega_2^2)} \, T \,, \quad \langle x^2 - y^2 \rangle = \frac{(a^{(3)} - a)(\Omega_1^2 - \Omega_2^2)}{a(a + a^{(3)})(aa^{(3)} + \Omega_1^2 + \Omega_2^2)} \, T \,, \tag{44}$$

$$R^2 = \langle x^2 \rangle + \langle y^2 \rangle = \frac{(2aa^{(3)}(a + a^{(3)}) + (3a + a^{(3)})(\Omega_1^2 + \Omega_2^2)}{a(a + a^{(3)})(aa^{(3)} + \Omega_1^2 + \Omega_2^2)} \, T \,. \tag{45}$$

For $a^{(3)} = a$ one has $\langle xy \rangle = \langle x^2 - y^2 \rangle = 0$ and $R^2 = 2T/a$. In contradistinction to the other couplings discussed above, this bi-rotational coupling does not affect these averages as long as the shear rate Γ is zero. In the following, we shall focus our attention on this case where the presence of the coupling with the "hidden" variable x_3 is not obvious in equilibrium when $\Gamma = 0$. As a side remark, we notice that $\langle x^2 - y^2 \rangle = 0$ und $\langle xy \rangle \geq 0$ for $a^{(3)} \geq a$ and $\Omega_1 \, \Omega_2 > 0$, provided that $\Omega_1^2 = \Omega_2^2$ applies.

The various coupling schemes discussed here are sketched in Fig. 1. The flow-induced couplings, shown in the top row, can be combined with any of the schemes indicated in the bottom row. The specific results to be presented in the following correspond to the combination of the plane Couette flow (top left) with the bi-rotational flow (bottom right).

Next, trajectories, density plots and the averages are displayed as functions of the shear rate. In order to point at the influence of the internal variable with bi-rotational coupling, the case without the coupling is considered first.

3.2. Two-dimensional harmonic oscillator, localized Brownian motion. Results for the isotropic two-dimensional oscillator, subjected to a plane Couette flow are presented next before the effect of the coupling with the internal variable is analyzed. Here the stationary state is stable for all shear rates, thus the trapped particle remains localized. This is in contradistinction to the case studied below in Sec. **3.3**. First, some remarks on the relevant bilinear averages are in order.

3.2.1. *Bilinear averages, flow alignment angle and trajectories.* With $x_1 = x$ and $x_2 = y$, the bilinear averages characterizing the behavior of the particle in the x, y-plane, are denoted by

$$R^2 = \langle x^2 \rangle + \langle y^2 \rangle \,, Q_+ = 2\langle xy \rangle \,, Q_- = \langle x^2 \rangle - \langle y^2 \rangle \,, Q^2 = Q_+^2 + Q_-^2 \,. \tag{46}$$

The flow alignment angle χ whose meaning shall be elucidated below, is determined by

$$\tan(2\chi) = \frac{Q_+}{Q_-} \,. \tag{47}$$

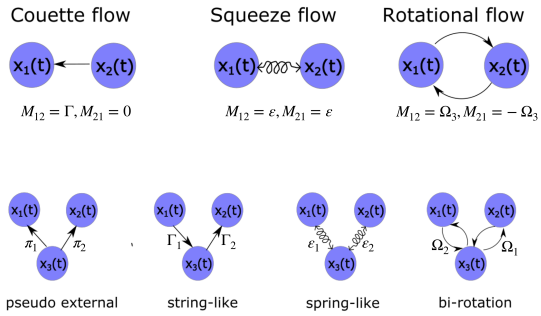

FIGURE 1. Schematic diagram for the coupling schemes. The top row indicates the coupling between x_1 and x_2 as it occurs in plane Couette, squeeze and rotational flow. The coupling of the auxiliary variable x_3 with x_1 and x_2 is sketched in the bottom row for pseudo external coupling, the string like and spring like chains as well as for the bi-rotational coupling scheme.

Flow-induced alignment of rod-like particles is observed by *flow-birefringence*, also called *streaming double refraction* (Maxwell 1874; Janeschitz-Kriegl 1983; Fuller 1995; Hess 2015). Its phenomenological description is analogous that one used here. The stationary solution of the relaxation equations (29), for $a^{(1)} = a^{(2)} = 1$ and $T = 1$ yields

$$\begin{gathered} Q_+ = (1 - M_{12}M_{21})^{-1}(M_{12} + M_{21}), \quad Q_- = (1/2)(M_{12} - M_{21})\,Q_+, \\ R^2 = 2 + (1/2)(M_{12} + M_{21})\,Q_+. \end{gathered} \tag{48}$$

These results are still exact. For the Couette flow with $M_{12} = \Gamma$, $M_{21} = 0$, we have

$$Q_+ = \Gamma, \quad Q_- = (1/2)\Gamma^2, \quad R^2 = 2 + (1/2)\Gamma^2, \quad Q = \Gamma\sqrt{1 + \Gamma^2/4}. \tag{49}$$

The corresponding quantities computed by Brownian dynamics simulations agree very well with these analytic results. Next have a look at Fig. 2 where the Brownian dynamics trajectory of the colloidal particle is presented for a Couette flow with the shear rate $\Gamma = 1.0$, as indicated at the top of the figure. The thick line indicates the theoretical alignment angle, given by

$$\tan(2\chi) = \frac{Q_+}{Q_-} = \frac{2}{\Gamma}. \tag{50}$$

The slope of the thin line is inferred from the values for Q_+, Q_-, computed in the Brownian dynamics simulation, with the help of

$$\tan(\chi) = \sin(2\chi)/(1 + \cos(2\chi)) = Q_+/(Q + Q_-), \quad Q = \sqrt{Q_+^2 + Q_-^2}. \tag{51}$$

For longer run times, the "experimental" slope approaches the theoretical one even better, but we preferred to show the present case in order to indicate that independent "data" determine the slopes of the thin and the thick lines. Clearly, the flow is towards the right

in the upper half of the xy-plane, and towards the left in the lower one, thereby imposing a preferential direction on the trajectory. This average alignment is characterized by the angle χ, which starts at 45 degrees for small shear rates. For larger values of Γ this angle becomes smaller, it tends closer towards the flow direction.

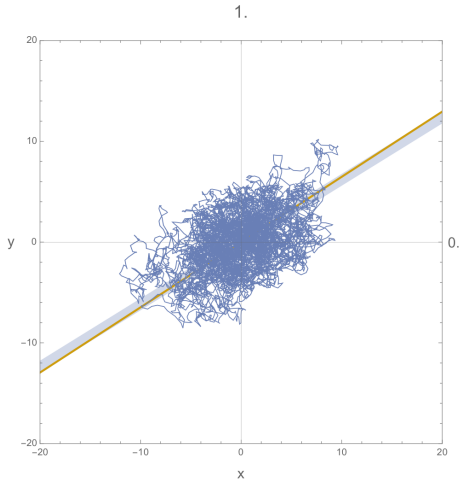

FIGURE 2. The Brownian dynamics trajectory of the colloidal particle in the presence of a Couette flow with the shear rate $\Gamma = 1.0$, recorded over 10^4 time steps of length $1.04/100 \approx 1/100$. The temperature is $T = 8$ corresponding to $R_{eq} = 4$. The thick line indicates the theoretical alignment angle. The slope of the thin line is inferred from Q_+, Q_-, as computed in the Brownian dynamics simulation.

3.2.2. *Probability density.* Next, the probability density (30) is specified for $n = 2$. The inverse of the matrix $((A_{11},A_{12}),(A_{21},A_{22}))$ is $((A_{22}/\det A, -A_{12}/\det A),(-A_{21}/\det A), A_{11}/\det A)$, with $\det A = A_{11}A_{22} - A_{12}A_{21}$. Recalling from equation (31): $A_{ij} = \delta_{ij} + \frac{n}{R^2} Q_{ij}$, $Q_{ij} = \langle x_i x_j \rangle - \frac{R^2}{n}\delta_{ij}$, and with $Q^*_{..} = Q_{..}/R^2$, we have $A_{11} = 1 + Q^*_-$, $A_{22} = 1 - Q^*_-$, $A_{12} = A_{21} = Q^*_+$, and $\det A = 1 - (Q^*_+)^2 - (Q^*_-)^2 = 1 - (Q^*)^2$. Thus (30) implies

$$\rho \sim \exp\left[-\frac{1}{R^2 \det A}\left[(x^2+y^2) - Q^*_+ 2xy - Q^*_-(x^2-y^2)\right]\right], R^2 \det A = R^2(1-(Q^*)^2) > 0\,. \tag{52}$$

For plane polar coordinates r and φ where $x = r\cos\varphi$, $y = r\sin\varphi$, $r^2 = x^2 + y^2$, we have

$$2xy = r^2 \sin(2\varphi)\,, \quad x^2 - y^2 = r^2\cos(2\varphi)\,. \tag{53}$$

Similarly, Q_+ and Q_- are expressed in terms of $Q = \sqrt{Q_+^2 + Q_-^2}$ and the flow alignment angle χ by

$$Q_+ = Q\sin(2\chi)\,, Q_- = Q\cos(2\chi)\,. \tag{54}$$

Then (52) can be rewritten as

$$\rho \sim \exp\left[-\frac{r^2}{R^2(1-(Q^*)^2)}\left[1-Q^*\cos\left(2(\chi-\varphi)\right)\right]\right], \quad Q^* = Q/R^2\,. \tag{55}$$

The maximal and minimal values $R^2_{max} = \langle r^2\rangle_{max}$ and $R^2_{min} = \langle r^2\rangle_{min}$ of the average squared distance $\langle r^2\rangle$, reached for $\varphi = \chi$ and $\varphi = \chi + \pi/2$, are given by

$$\frac{R^2_{max/min}}{R^2} = 1 \pm Q^*\,. \tag{56}$$

Since

$$\frac{R^2_{max} - R^2_{min}}{R^2_{max} + R^2_{min}} = Q^*\,, \tag{57}$$

the quantity Q^*, defined above, is a measure for the eccentricity. The standard "numerical eccentricity" e of an ellipse is defined as the ratio of the distance between the foci, divided by the long axis. It is related to Q^*, by $e^2 = (R^2_{max} - R^2_{min})/R^2_{max} = 2Q^*/(1+Q^*)$. The quantity $Q^* \neq 0$ is responsible for the "deformation" of the particle clouds seen in the following contour plots. For the plane Couette flow with the shear rate Γ, the eccentricity Q^* and the flow alignment angle χ are given by

$$Q^* = \frac{\Gamma}{\sqrt{4+\Gamma^2}}\,, \quad \tan(2\chi) = 2/\Gamma\,. \tag{58}$$

In the following graphs, the probability density is represented by dots which mark the positions of the particle in the Brownian dynamics simulation. The contours are generated with the help of (52) where the parameters R^2, Q_+, Q_- are calculated as averages in the Brownian dynamics, over the same run time. Examples are displayed in Figs. 3 and 4. As for Fig. 2, the data are recorded over 10^4 time steps of length $1/100$, the temperature is $T = 8$ corresponding to $R_{eq} = 4$. The numbers on top of the graphs indicate the imposed shear rate, those on the right stand for the number of transits which are non-zero only for the source-sink flow situation considered in the following section. "Bright" and "dark" correspond to high and low values of the probability density. The data points cluster in the region of the high probability. With increasing shear rate the long axes of the contour ellipses are tilted stronger in the flow direction, which is towards the right, for $y > 0$ and towards the left, for $y < 0$. The results of this section are in accord with those presented by Bammert and Zimmermann (2010). Next, consequences of the coupling with the internal variable are analyzed.

3.3. From localized Brownian motion to source-sink flow, $n = 3$.

3.3.1. *Auxiliary variable with bi-rotational coupling and delocalization.* We now consider the extented system with one auxiliary variable as introduced in Sec. **3.1.4**. In the absence of a shear flow in the x_1x_2-plane, corresponding to the shear rate $\Gamma = 0$, the averages $\langle x_1x_2\rangle$ and $\langle x_1^2\rangle - \langle x_2^2\rangle$ are zero, just as in an ordinary equilibrium state, when the coupling of the x_1x_2 harmonic oscillator with the auxiliary variable x_3 is of bi-rotational type. Of course, $\Gamma \neq 0$ leads to $\langle x_1x_2\rangle \neq 0$ and $\langle x_1^2\rangle - \langle x_2^2\rangle \neq 0$ with a shear rate dependence of these quantities

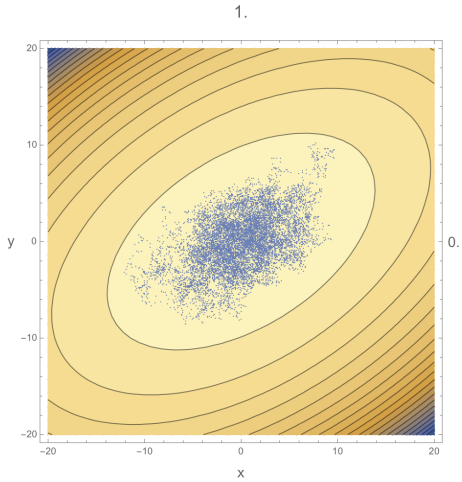

FIGURE 3. Density cloud of the colloidal particle and contour plot of the probability distribution, for a Couette flow with the shear rate $\Gamma = 1.0$ and with the same parameters as in Fig. 2. The contour curves are obtained from (52) with R^2, Q_+, Q_-, computed in the Brownian dynamics simulation, which also yields the points shown.

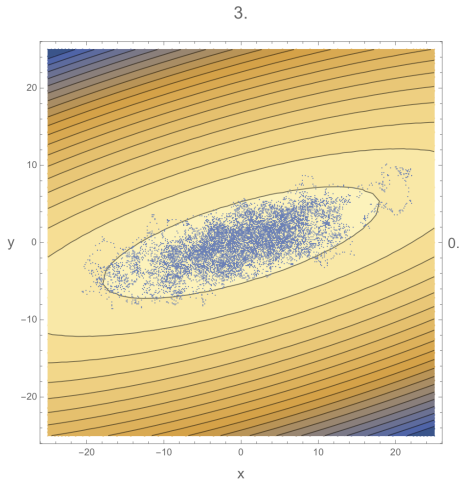

FIGURE 4. Contour plot of the probability distribution and density of the colloidal particle, for a Couette flow with the shear rate $\Gamma = 3.0$. The contour curves are obtained from (52) with R^2, Q_+, Q_-, computed in the Brownian dynamics simulation, which also yields points for the positions of the particle.

which differs from that without the coupling to the auxiliary variable. Interestingly, this difference is not only quantitative but can also be of qualitative type, like a transition from

a steady state to an instationary state corresponding to a delocalization of the particle or an escape from the trap. It should be stressed, here the term "escape" does not refer to the motion of a particle over a potential barrier, but rather to a flow induced transition from a stable stationary state, of overdamped oscillatory type around the position $x = 0$, to a transient state. This occurs abruptly, like in a second order phase transition, when the imposed steady shear rate exceeds a critical value Γ_{crit}. Left alone, the particle would escape with an exponentially growing distance from the center $x = 0$. In the simulation, this leads to numerical overflow. The overflow is avoided by catching and removing the particle from the system at a finite distance. The particle can be reinserted at the origin, in a rapid transit, after one time step. Then one is dealing with a "source-sink" set up, where again a stationary state can be reached. With this regularization or "taming" of the dynamics, trajectories, density plots and averages can be computed for shear rates above the critical value just as well as below. For $\Gamma > \Gamma_{crit}$, an additional quantity of interest is the number of transits from the origin to the outer rim which can be counted and divided by the total run time to yield the transit rate ν_{trs}. Close to and above the transition, ν_{trs}.increases proportional to $\Gamma - \Gamma_{crit}$.

Some remarks on the source-sink flow are added. The source is at the center $x = 0$, the sink is at the surface which is the maximum distance R_m away from the center, where $R_m^2 = x^2 + y^2$. Notice that the auxiliary variable x_3 is not involved in this definition. The value of R_m should be larger than the average distance from the center in equilibrium. Typically we choose $R_m^2 = 10^2$ to 10^6 times $\langle x^2 + y^2 \rangle_{eq}$. When the particle reaches the outer rim of the allowed domain, it is transferred to the center within 1 time step δt. This means an extra contribution $R_m/\delta t$ to the raw data which yield the average velocity.

3.3.2. *Trajectories and probability density.* Here trajectories, density clouds and contour plots of the probability density are displayed in the xy-plane, corresponding to $x_3 = 0$. Thus traces of the "hidden" internal variable are not detected directly, but it does affect the x_1, x_2-dynamics which we record in the xy-plane. We recall that the strength of coupling of x_1 and x_2 to the auxiliary variable is quantified by the parameters Ω_1 and Ω_2. First a trajectory is shown in Fig. 5 for a Couette flow with the shear rate $\Gamma = 2.0$, as indicated at the top of the figure, for a bi-rotational coupling with the auxiliary variable where $\Omega_1 = \Omega_2 = 1$, computed over 10^4 time steps of length $1/100$. The temperature is $T = 8$, thus $R_{eq} = 4$, as for the figures above. The thin line indicates the flow alignment angle, as inferred from the BD simulation. Its slope agrees well with the appropriate theoretical line. In order to reveal the effect of the internal variable, however, the thick line shows the corresponding theoretical result for the flow alignment angle obtained without the coupling to x_3, *i.e.* $\Omega_1 = \Omega_2 = 0$. The internal variable seems to exert an extra resistance against tilting the trajectory towards the flow direction. The same applies to the contour plots presented below.

Next density clouds and contour plots of the probability density are presented. For Fig. 6 the same parameters are used as for Fig. 5. It is recalled that the numbers on top of the graphs indicate the imposed shear rate, those on the right stand for the number of transits which are non-zero only for the source-sink flow situation considered below. "Bright" and "dark" correspond to high and low values of the probability density. The data points cluster in the region of the high probability.

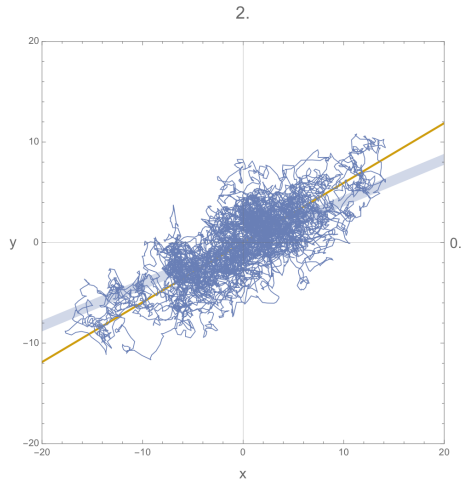

FIGURE 5. The Brownian dynamics trajectory of the colloidal particle, in the presence of a Couette flow with the shear rate $\Gamma = 2.0$, for a bi-rotational coupling with the auxiliary variable where $\Omega_1 = \Omega_2 = 1$. The thick line indicates the theoretical alignment angle without taking the coupling into account ($\Omega_1 = \Omega_2 = 0$). The slope of the thin line is inferred from Q_+, Q_-, as computed in the Brownian dynamics simulation.

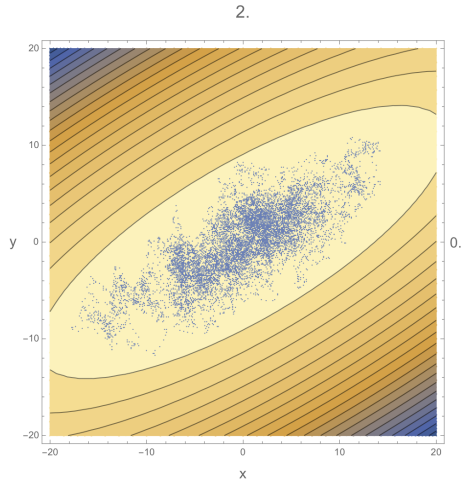

FIGURE 6. Contour plot of the probability distribution and density of the colloidal particle, for a Couette flow with the shear rate $\Gamma = 2.0$, for a bi-rotational coupling with the auxiliary variable where $\Omega_1 = \Omega_2 = 1$. The contour curves are obtained from (52) with R^2, Q_+, Q_-, computed in the Brownian dynamics simulation, which also yields points for the positions of the particle.

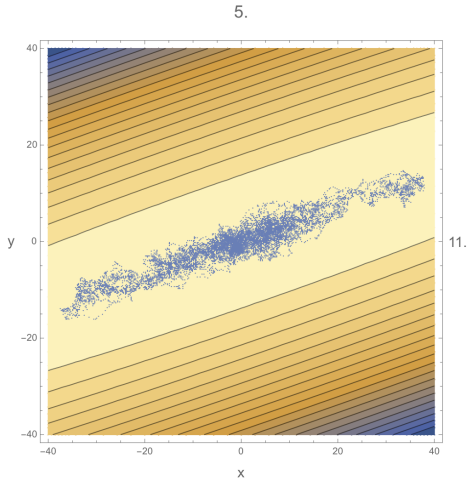

FIGURE 7. Contour plot of the probability distribution and density of the colloidal particle, for a Couette flow with the shear rate $\Gamma = 5.0$, for a bi-rotational coupling with the auxiliary variable where $\Omega_1 = \Omega_2 = 1$. The contour curves are obtained from (52) with R^2, Q_+, Q_-, computed in the Brownian dynamics simulation, which also yields points for the positions of the particle.

Figure 7 presents an example for density clouds and contour plots for shear rates beyond the critical shear rate $\Gamma_{crit} = 3$, where a stationary state can be approached in a source-sink set up. The density is still tilted in the flow direction, yet it is extremely elongated, with an almost cylindrical shape. The maximum extension is determined by $R_m = 40$. The number on the right of the graph indicates the transits from the center to the rim at $r^2 = R_m^2$ during the run time.

3.4. Analytic Solutions for steady state averages and comparison with BD data.

3.4.1. *Explicit analytic solutions.* Next, the analytic solutions of the relaxation equations for the averages of the bi-llnear quantities $r^2 = x^2 + y^2, xy, x^2 - y^2$ are stated explicitly, as functions of the shear rate $\Gamma \geq 0$, for the special case $a^{(3)} = a$ and $\Omega_1 = \Omega_2 = \Omega$. The following section is then devoted to the comparison with results computed via BD simulations. The expressions of interest are

$$\langle xy \rangle = Q_+/2 = \frac{\Gamma}{a} \frac{H^{(1)}}{\mathscr{D}} \frac{T}{a}, \quad H^{(1)} = a^{-4} \left(4a^4 + 8a^2 \Omega^2 + 3\Omega^4 - a\Gamma\Omega^2\right), \tag{59}$$

$$Q_- \equiv \langle x^2 \rangle - \langle y^2 \rangle = \frac{\Gamma^2}{a^2} \frac{H^{(2)}}{\mathscr{D}} \frac{T}{a}, \quad H^{(2)} = a^{-3} \left(4a^3 + 5a\Omega^2 - \Gamma\Omega^2\right), \tag{60}$$

and

$$R^2 = \langle x^2 \rangle + \langle y^2 \rangle = \frac{H^{(0)}}{\mathscr{D}} \frac{T}{a}, \tag{61}$$

with

$$H^{(0)} = a^{-5}\,(16a^5 + 40a^3\Omega^2 + 16a\,\Omega^4 - \Gamma\,(10a^2\Omega^2 + 2\Omega^4) + \Gamma^2(4a^3 + 5a\,\Omega^2) - \Gamma^3\,\Omega^2)\,, \tag{62}$$

where

$$\mathscr{D} = a^{-6}\,(a^3 + 2a\,\Omega^2 - \Gamma\,\Omega^2)(8a^3 + 4a\,\Omega^2 + \Gamma\,\Omega^2)\,. \tag{63}$$

Notice: the determinant $\mathscr{D}$ becomes zero for the critical shear rate Γ_{crit} determined by

$$\Gamma_{crit}/a = 2 + a^2/\Omega^2\,. \tag{64}$$

The corresponding determinant $\det(K)$, see (37), also vanishes at the same shear rate. For $a = 1$ and $\Omega = 1$ we have $\Gamma_{crit} = 3$.

3.4.2. *Averages of* $r^2\,, xy\,, x^2 - y^2$. The BD simulations were performed for $a = 1, \Omega = 1, T = 1$ with the time step $\delta t = 0.104$, the critical shear rate is $\Gamma_{crit} = 3$. The limiting radius is $R_m = 40$. For $\Gamma > \Gamma_{crit}$ the particle is set back to the origin when it reaches $r^2 = R_m^2$. The data are extracted over the run time $t_{run} = 1040$ corresponding to 10000 time steps. The comparison with the stationary solutions of the relaxation equations, as presented in the previous section is physically meaningful for shear rates below the singularity at Γ_{crit}. In some cases, however, it may be of interest to inspect also the analytic solutions for $\Gamma > \Gamma_{crit}$. First $R^2 = \langle x^2\rangle + \langle y^2\rangle$ is plotted in Fig. 8 as function of the shear rate. The data points

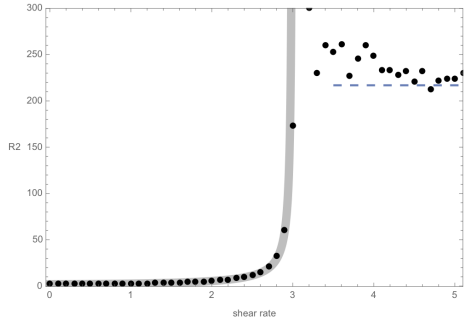

FIGURE 8. The square of the mean radius $R^2 = \langle x^2\rangle + \langle y^2\rangle$, as function of the shear rate. The black points stem from the BD simulations. The thick line follows from the stationary solution of the relaxation equations. The model parameters are $a = 1, \Omega = 1, T = 1, R_m = 40$, the critical shear rate is $\Gamma = 3.0$. The dashed horizontal line marks an estimate for R^2 in the trans-critical region, cf. Sec. **3.4.3**.

are computed in the BD simulations, the thick curve indicates the analytic result with the singularity at Γ_{crit}. The data points for $\Gamma > \Gamma_{crit}$ stem from the source-sink set up, which is dormant as long as the outer rim of the allowed domain with radius R_m is not reached. The scatter of the data points is due to the fact that the run time used is not long enough to yield a sufficiently large number of transits, from the center to the rim, in order to reach a steady state behavior. For the number of transits see Fig. 11. The dashed horizontal line marks the estimate $R^2 \approx R_m^2/\ln(R_m^2)$ for the trans-critical region, see Sec. **3.4.3**. The increase of R^2 by over two orders of magnitude in the pre-critical region is a clear indicator of the

singularity predicted by the analytic solutions of the relaxation equations. Just as in real physical systems, the BD simulations are regularized such that the computed data are finite numbers.

Next, results are presented in Figs. 9 and 10 for $\langle xy \rangle$ and $Q_m \equiv Q_- = \langle x^2 \rangle - \langle y^2 \rangle$.

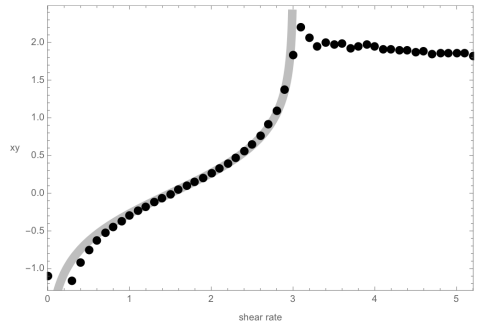

FIGURE 9. The average $\langle xy \rangle$, as function of the shear rate. The black points stem from the BD simulations. The thick line follows from the stationary solution of the relaxation equations. The model parameters are $a = 1, \Omega = 1, T = 1$, and $R_m = 40$, the critical shear rate is $\Gamma = 3.0$. A logarithmic scale is used for the vertical axis.

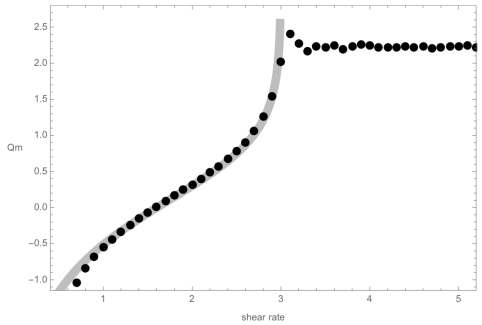

FIGURE 10. The quantity $Q_m \equiv Q_- = \langle x^2 \rangle - \langle y^2 \rangle$, as function of the shear rate. The black points stem from the BD simulations. The thick line follows from the stationary solution of the relaxation equations. The model parameters are $a = 1, \Omega = 1, T = 1$ and $R_m = 40$, the critical shear rate is $\Gamma = 3.0$. A logarithmic scale is used for the vertical axis.

Between $\Gamma = 0.3$ and 3, these quantities increase by three orders of magnitude, Notice the logarithmic scale used for the vertical axis. Again the thick curve marks the analytic results.

A word of caution is in order for the comparison of simulation data with the analytical results. The smaller the shear rates, the longer are the run times required to achieve a satisfactory signal-to-noise ratio for the computed averages. This is well known from

NEMD simulations (Evans *et al.* 1984). For the parameters used here, typically 10^4 time steps are sufficient for Γ larger than about 0.3.

A quantity which indicates the critical shear rate in an impressive way and the apparent continuity of some observables across the singularitiy is discussed in the Appendix.

3.4.3. *Number of transits and scaled transit rate.* The number of transits between the center and the rim can be counted and recorded as function of the shear rate, this number is called N_{tr}. An example is shown in Fig. 11. The model parameters are the same as those used

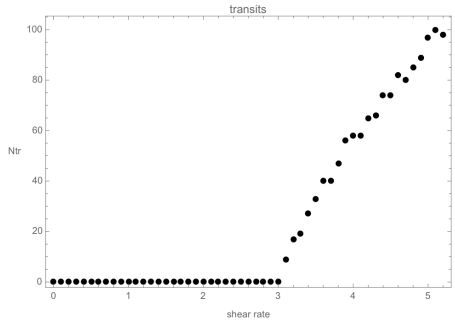

FIGURE 11. The number of transits N_{tr} of the particle, from the center to the rim, as function of the shear rate, as observed in the BD simulations, over 10^4 time steps. The model parameters are $a = 1$, $\Omega = 1$, $T = 1$ and $R_m = 40$.

for the three previous graphs. The number of transits N_{tr}, divided by the run time t_{run} is the *transit rate* $\nu_{trs} = N_{tr}/t_{run}$. It seems plausible that ν_{trs} is smaller for larger R_m. Scaling arguments applied to the Smoluchowski equation for the source-sink set up suggest a scaling with R^2/R_m^2. So it is expected that the scaled transit rate ν^*_{trs}, defined by $\nu^*_{trs} \sim (R_m^2/R^2)\,\nu_{trs}$, be independent of R_m, within computational accuracy. The numerical factor is specified below. We found that the scaling relation is indeed obeyed for $R_m = 20, 40, 80$ with $a = 1, \Omega = 1, T = 8$, corresponding to $R_{eq} = 4$, where $R_{eq}^2 = \langle x^2 + y^2 \rangle_{eq}$, as well as for $R_m = 40, 100$ and 1000 with $a = 1, \Omega = 1, T = 1$ corresponding to $R_{eq} = 2^{1/2}$, and for the shear rates between $\Gamma_{crit} = 3$ and 5.3. The following considerations imply that the scaled transit rate is determined by the largest, positive eigenvalue λ of the determinant associated with the relaxation equations governing the linear averages (26). For our set up, the eigenvector pertaining to the positive eigenvalue is parallel to the direction specified by the flow alignment angle. Let the component parallel to this direction be denoted by X. Its time dependence is given by $X(t) = X_0 \exp(\lambda t)$ with $X_0 = X(0)$. Assuming that this component dominates all other contributions to the square of the position vector, we have $r^2 = x^2 + y^2 \approx X_0^2 \exp(2\lambda t)$. The transit time t_{trs} is determined by $R_m^2 = X_0^2 \exp(2\lambda\, t_{trs})$. We identitfy $R^2 = \langle r^2 \rangle$ with the time average of $X(t)^2$, from $t = 0$ to $t = t_{trs}$, thus

$$t_{trs} R^2 = \int dt X(t)^2 = X_0^2 (2\lambda)^{-1} (\exp(2\lambda) - 1) = (2\lambda)^{-1} (R_m^2 - X_0^2)\,. \tag{65}$$

It is understood that X_0^2 should be replaced by an average value, not larger than the equilibrium value $\langle x^2 \rangle_{eq}$, which, in turn, should be small compared with R_m^2. Thus one obtains for the transit rate $\nu_{trs} = (t_{trs})^{-1} = 2\,\lambda\,(R^2/R_m^2)$, which yields for the scaled transit rate

$$\nu_{trs}^* \equiv (1/2)(R_m^2/R^2)\,\nu_{trs} = \lambda\,. \tag{66}$$

In the simulations, this relation is obeyed very well. An example is shown in Fig. 12 where the scaled transit rate is plotted as function of the shear rate. The model parameters are

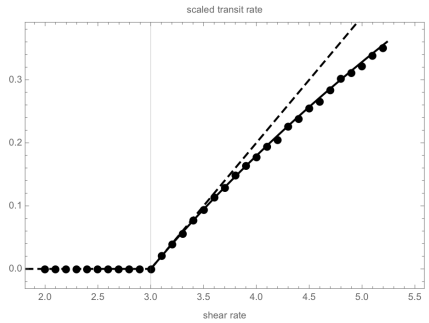

FIGURE 12. The scaled transit rate, as function of the shear rate. The points stem from the BD simulations. The model parameters are $a = 1$, $\Omega = 1$, $T = 1$ and $R_m = 100$. The curve shows the largest eigenvalue λ as function of the shear rate, cf. Equation (66). The dashed line corresponds to $(\Gamma - \Gamma_{crit})/5$.

$a = 1$, $\Omega = 1$, $T = 1$ and $R_m = 100$. The points shown stem from the BD simulations, averaged over 10^4 time steps equivalent to a run time of 10^3. The curve corresponds to $\lambda = \lambda(\Gamma)$, as determined by the eigenvalue equation

$$\Gamma - 3 = 5\lambda + 3\lambda^2 + \lambda^3\,, \tag{67}$$

for $\Gamma > \Gamma_{crit} = 3$. A parametric plot was used to generated the curve in Fig. 12. The dashed line corresponds to $(\Gamma - \Gamma_{crit})/5$. The considerations presented above imply

$$R^2 = (2\,\lambda t_{trs})^{-1}(R_m^2 - X_0^2) = ((R_m^2 - X_0^2)/\ln(R_m^2/X_0^2) \approx R_m^2/\ln(R_m^2/X_0^2)\,. \tag{68}$$

For $X_0^2 = 1$ this is the value used in Fig. 8. as an estimate for R^2 in the trans-critical region.

4. Concluding remarks

The simple model system of an overdamped harmonic oscillator, subjected to fluctuating forces, where the first n_{obs} of its n components are associated with the observable variables and the remaining $n_{int} = n - n_{obs}$ components are treated as "internal" or auxiliary variables, can show rather complex dynamic behavior. As demonstrated here, this applies even for $n_{obs} = 2$ and $n_{int} = 1$, when the uncoupled components describe an equilibrium state and non-diagonal coupling drives the system into non-equilibrium. More specifically, the coupling between the two observable components is associated with a shear flow and the

remaining four coupling coefficients are chosen such that this coupling is "hidden" as long as the the shear rate is not turned on. The coupling with the internal variable not only affects the shear rate dependence of observable quantities, such as trajectories, the probability density and averages, in a quantitative manner. Intriguingly, it also gives rise to a transition from a stationary non-equilibrium state to an transient instationary state, when the shear rate exceeds a critical value.

The forces linear in the components of the position vector imply that the averages of expressions bilinear in the components obey a closed set of relaxation equations which possesses stationary solutions whose highly non-linear dependence on the coupling coefficients is known and can be compared with numerical data from Brownian dynamics simulations. Furthermore, the probability density is Gaussian and it is characterized by its second moments which are the bilinear averages, even in stationary non-equilibrium states. The tools used here, the Brownian dynamics simulations and solutions of the Smoluchowski equation, can also be applied to systems with a more general potential function governing the equilibrium density. This applies also to the effective two-particle potential associated with the equilibrium radial distribution function when the density distribution is identified with the pair-correlation function, as suggested by Kirkwood (1946). Then the relaxation equations for the second moments are coupled with those of higher moments and the density distribution is no longer Gaussian. The theoretical analysis becomes more involved, approximations have to be made and their limits of applicability have to be tested. The appeal of exact solutions available for linear forces, however, is lost.

With appropriate modifications and re-interpretations, the analytical and numerical results obtained here for a colloidal particle in a trap can be applied to polymer molecules in a dilute solution. The trajectories can be interpreted as folded polymer chains, the density clouds may represent the beads of the polymer. Such analogies are well established (*e.g.*, see Doi and Edwards 1986). Our studies can provide results for several phenomena.

(i) Shear-flow-induced deformation and orientation of polymer molecules (Janeschitz-Kriegl 1983; Fuller 1995). Experimentally, these effects can be detected in flow-birefringence measurements, which *e.g.* yield the flow alignment angle, as well as via light scattering and small angle neutron scattering (SANS) experiments which measure the spatial Fourier transform of the probability density. It is also determined by the bilinear averages.

(ii) Oscillator-dumbbell, also called elastic-dumbbell model, for rheological properties (Doi and Edwards 1986). The shear-rate dependence of the polymer contribution to the viscosity and to the first normal stress difference can be inferred from results obtained for the bilinear averages $\langle xy \rangle$ and $\langle x^2 - y^2 \rangle$.

(iii) Coil-stretch transition (de Gennes 1974; Larson and Magda 1989). This effect is analogous to shear-flow induced delocalization transition studied here. The applications to polymer molecules deserve more attention but are beyond the scope of this article.

A further interesting direction for future research is to analyse the systems and phenomena studied here from a non-equilibrium thermodynamics point of view. For example, what is the impact of the auxiliary variable(s) on a suitably defined distance from equilibrium and on measures of irreversibility? We note that similar questions have also been addressed for systems with one physical degree of freedom (Loos and Klapp 2020) and for underdamped

model systems (see Netz 2020). For the present, shear-driven colloidal system, such an investigation could be done on the ensemble-averaged level, *e.g.*, via the entropy production defined in (17), but also on the level of the noisy trajectories using tools from stochastic thermodynamics (Seifert 2005, 2012; Loos and Klapp 2020). Work in these directions is desirable and in preparation.

Acknowledgements

This work has been performed under the auspices of the Collaborative Research Center SFB 910 "Kontrolle selbstorganisierender nichtlinearer Systeme: Theoretische Methoden und Anwendungskonzepte" (Control of self-organizing nonlinear systems: Theoretical methods and concepts of application). We thank the Deutsche Forschungsgemeinschaft (DFG, German Research Foundation) for financial support via project number 163436311 - SFB 910. We thank a referee for helpful comments and for having drawn our attention to the studies of the Brownian gyrator.

Appendix A.

A.**1. Computational details of BD simulations.**

A.**1.1.** *Integrators.* First some remarks are made on the simple explicit *Euler method.* Now x_n stands for $x(t_n)$ with $t_n = n\,h_s$, $n = 1,2,\ldots,N_{run}$ where h_s is the length of a time step and N_{run} is the number of time steps in one simulation run, the run time is $t_{run} = N_{run}\,h$. Here the subscript n indicates a the discrete time variable, not a component of the vector x. The simple explicit Euler method for integration for the differential equation $dx/dt = v(x,\zeta)\,, \quad v = F(x(t)) + \zeta\,$, is

$$x_{n+1} = x_n + h_s\,v_n\,, \quad v_n = F(x_n) + \zeta_n\,, \tag{69}$$

where ζ is the fluctuating force and ζ_n is the corresponding n-th random number. The first step $x_1 = x_0 + v_0 h_s$ requires the specification of the starting values x_0, v_0. The unbiased choice $x_0 = 0\,, v_0 = 0$ can be made, it implies $x_1 = h_s\,\zeta_1$. We tested both the simple explicit Euler method as well as a modified Euler method. The latter one is akin to the Störmer-Verlet method (Verlet 1967). Two half-step midpoint Euler steps are involved where the forces are computed just once per step, but the length h of the time step is twice that of the simple Euler method. This modified Euler method works as follows. Given

$$v_{n-1} = F(x_{n-1/2}) + \zeta_{n-1} \tag{70}$$

from the previous time step, the first half-step is

$$x_{n+1/2} = x_n + (h/2)\,v_{n-1}\,. \tag{71}$$

Next v_n is computed according to

$$v_n = F(x_{n+1/2}) + \zeta_n\,. \tag{72}$$

The second half-step yields x_{n+1}:

$$x_{n+1} = x_{n+1/2} + (h/2)\,v_n\,. \tag{73}$$

Thus we have

$$x_{n+1} - x_n = (h/2)\left(F(x_{n-1/2}) + F(x_{n+1/2})\right) + (h/2)(\zeta_{n-1} + \zeta_n)\,. \tag{74}$$

For comparison, the difference between $x_{n+1} - x_{n-1}$ pertaining to the simple Euler method with time step h_s is stated:

$$x_{n+1} - x_{n-1} = h_s\,(F(x_{n-1}) + F(x_n)) + h_s(\zeta_{n-1} + \zeta_n)\,. \tag{75}$$

With $h_s = (h/2)$, the terms involving the random force ζ are equivalent. This is not the case for the terms containing the continuous force F. Since $F(x_{n\pm1/2}) = F(x_n) \pm (h/2)v_n F'(x_n) + (1/2)(h/2)^2 v_n^2 F''(x_n) + \ldots$, where F' and F'' indicate the first and second spatial derivatives of F, we have $F(x_{n-1/2}) + F(x_{n+1/2}) = 2F(x_n) + O(h^2)$. The computational error of the modified Euler method is of the order h^3 times the second derivative F'' of F, which vanishes for linear forces. The situation is different for the simple Euler method. Since $F(x_{n-1}) = F(x_n) - h_s v_n F'(x_n) + \ldots$, we have $F(x_{n-1}) + F(x_n) = 2F(x_n) + O(h_s)$. The computational error of the simple explicit Euler method is of the order $h_s^2 \sim h^2$ times the first derivative F' of F, which is non-zero even for linear forces.

A.**1.2.** *Time step for the overdamped harmonic oscillator.* A criterion to determine the time step h_s is the condition that the mean value of x^2, in equilibrium, should have the prescribed value. We want to choose the step size h_s adequate for the force $F = -x$, and for the case where the time average $\overline{x^2}$ is 1 and the average of the pertaining noise $\overline{\zeta^2}$ is 2, pertaining to $T = 1$. The simple Euler iteration method (69) corresponds to

$$x_{n+1} - x_n = (-x_n + \zeta_n)\,h_s\,. \tag{76}$$

Taking the square on both sides yields $(x_{n+1} - x_n)^2 = (-x_n + \zeta_n)^2\,h_s^2$, and consequently $x_{n+1}^2 + x_n^2 - 2x_{n+1}x_n = x_n^2 + \zeta_n^2 - 2x_n\,\zeta_n$. Now both sides are averaged. We use $\overline{x^2} = \frac{1}{N}\sum_{n=1}^{N} x_n^2$, The quantity C_1 is defined by $\frac{1}{N}\sum_{i=1}^{N} x_{n+1}x_n = C_1\overline{x^2}$. Here C_1 corresponds to the positional correlation time function $C(t)$ taken at the value $t = h_s$, thus $C_1 = C(h_s)$. Furthermore we use $(1/N)\sum_{n=1}^{N} x_n\zeta_n = 0$, since x_n depends only on previous fluctuation ζ_k, where $k = 1, \cdots n-1$, but not on ζ_n. Thus we obtain $2\overline{x^2}(1 - C_1) = h_s^2(\overline{x^2} + \overline{\zeta^2})$, or $1 - C_1 = (1/2)h_s^2(1 + \overline{\zeta^2}/\overline{x^2})$. The conditions $\overline{x^2} = 1$, $\overline{\zeta^2} = 2$ and $C(t) = e^{-t}$ lead to

$$1 - e^{-h_s} = \frac{3}{2}h_s^2\,, \quad h_s^2 = \frac{2}{3}(1 - e^{-h_s})\,. \tag{77}$$

From the approximation $e^{-h_s} \approx 1 - h_s + \frac{1}{2}h_s^2$ follows $h_s \approx \frac{1}{2}$. The numerical analysis yields $h_s = 0.52$. The corresponding step length for the modified Euler method is $h = 2h_s = h_0 \equiv 1.04$.

In applications it is desirable to use flexible, in general shorter time steps in order to obtain a finer resolution of the dynamics. At the same time, the equilibrium properties, like $\langle x^2\rangle_{eq}$ should retain their prescribed values. This is achieved by adjusting the strength of the fluctuating forces. Let the systematic force be $-a\,x$, the temperature T and the corresponding equilibrium average of x^2 is wanted to be $\langle x^2\rangle_{eq} = T/a$. Furthermore, the choice of the integration time step is $\delta t = h_0 t_{st}$, with the time stretch factor t_{st} typically

between $1/100$ and 1. Then the strength of the fluctuating force ζ is set as $\zeta = \sqrt{2\vartheta}\,\xi$ with $\overline{\xi^2} = 1$ and $\vartheta = T/t_{st}$. In the text, time steps $1.04 \times 1/10$ and $1.04 \times 1/100$ are also referred to as $1/10$ and $1/100$.

A.**2. Indicator for the critical shear rate.** The positional shift of $x(t)$, between two successive time steps, divided by its length δt, defines the x-component v_x of the velocity of the particle: $v_x = (x(t) - x(t-\delta t))/\delta t$. The average $\langle v_x^2 \rangle$, divided by the average of x^2, *i.e.* $vx2 = \langle v_x^2 \rangle / \langle x^2 \rangle$, is called reduced square of the x-velocity. When we plotted this quantity, we discovered by chance, that it is an excellent indicator for the critical shear rate. An example is presented in Fig. 13.

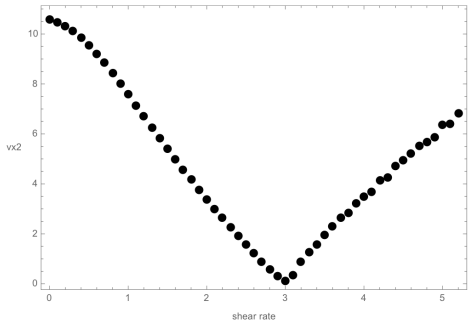

FIGURE 13. The reduced square of the x-velocity, $vx2 = \langle v_x^2 \rangle / \langle x^2 \rangle$, as function of the shear rate. The black points stem from the BD simulations with the model parameters $a = 1$, $\Omega = 1$, $T = 1$ and $R_m = 40$. The critical shear rate $\Gamma = 3.0$ is clearly indicated by the point where the first derivative of the "curve" has a discontinuity.

Why does this indicator work the way it does? The answer to this question is apparent from the behavior of its two factors $1/\langle x^2 \rangle$ and $\langle v_x^2 \rangle$, as functions of the shear rate. The first one decreases from $1/\langle x^2 \rangle_{eq}$ to very small, but finite values for $\Gamma \geq \Gamma_{crit}$, whereas the second one is small for $\Gamma \leq \Gamma_{crit}$, however, it increases strongly for $\Gamma > \Gamma_{crit}$, similarly to the number of transits N_{tr}. The reason is that the back-transit from the rim to the center, which happens within one time step, gives the large contribution of the order of $R_m/\delta t$, to the raw data for the velocity. Thus the product of $1/\langle x^2 \rangle_{eq}$ and $\langle v_x^2 \rangle$ yields the wedge-like dip at Γ_{crit}, as seen in Fig. 13.

A.**3. An apparent continuity across the singularity.** In the theoretical expression for the flow alignment angle χ, computed via the ratio Q_+/Q_-, the determinant $\mathscr{D}$ cancels and the singularity at Γ_{crit} does not show up. The same applies to the eccentricity Q^* and also to the prefactor $R^2 \det A$ which appears in (52). In contradistinction to the graphs displayed above in Sec. **3.4**, plots of these analytic functions continue smoothly into the region $\Gamma > \Gamma_{crit}$ where the stationary solution no longer exists. So one may wonder whether the corresponding data computed via Brownian dynamics, which agree well with the analytic results for $\Gamma < \Gamma_{crit}$ show a similar behavior. And indeed, for the particular model parameters considered above, the data points for the flow alignment angle continue smoothly

beyond the critical shear rate. However, further away from Γ_{crit} the BD data for χ become systematically smaller than the extension of the analytic curve, beyond the limit of its applicability. The behavior of the eccentricity Q^* is similar. Good agreement between numerical and analytic results is observed for $\Gamma \leq \Gamma_{crit}$. For $\Gamma > \Gamma_{crit}$, the analytic curve continues to values $Q^* > 1$, whearas the BD data stay close to, but below the physically maximal value $Q^* = 1$, without indicating any discontinuity at $\Gamma = \Gamma_{crit}$. Remarkable is the behavior of the quantity $R^2 \det A = R^2(1-(Q^*)^2)$ which occurs in the expression (52) for the probability density. The continuation of the analytic formulae beyond Γ_{crit} yield the physically not meaningful results $R^2 < 0$ and $(Q^*)^2 > 1$, yet the product $R^2(1-(Q^*)^2)$ remains positive and is continuous across the singularity. This is essential for the application of (52) both for shear rates above Γ_{crit}, just as for shear rates smaller than Γ_{crit}.

References

Allen, M. P. and Tildesley, D. J. (2017). *Computer Simulation of Liquids*. 2nd ed. Oxford University Press. DOI: 10.1093/oso/9780198803195.001.0001.

Bammert, J. and Zimmermann, W. (2010). "Probability distribution of a trapped Brownian particle in plane shear flow". *Physical Review E* **82**, 052102. DOI: 10.1103/PhysRevE.82.052102.

Brady, J. F. and Bossis, G. (1988). "Stokesian dynamics". *Annual Review of Fluid Mechanics* **20**(1), 111–157. DOI: 10.1146/annurev.fl.20.010188.000551.

Cerasoli, S., Dotsenko, V., Oshanin, G., and Rondoni, L. (2018). "Asymmetry relations and effective temperatures for a biased Brownian gyrator". *Physical Review E* **98**(4), 042149. DOI: 10.1103/PhysRevE.98.042149.

de Gennes, P. G. (1974). "Coil-stretch transition of dilute flexible polymers under ultrahigh velocity gradients". *Journal of Chemical Physics* **60**, 5030. DOI: 10.1063/1.1681018.

de Groot, S. R. and Mazur, P. (1962). *Non-Equilibrium Thermodynamics*. Amsterdam: North-Holland Publ. Co.

Doerries, T. J., Loos, S. A. M., and Klapp, S. H. L. (2021). "Correlation functions of non-Markovian systems out of equilibrium: Analytical expressions beyond single-exponential memory". *Journal of Statistical Mechanics: Theory and Experiment* **2021**(3), 033202. DOI: 10.1088/1742-5468/abdead.

Doi, M. (1980). "Rheological properties of rodlike polymers in isotropic and liquid crystalline phases". *Ferroelectrics* **30**, 247. DOI: 10.1080/00150198008209520.

Doi, M. and Edwards, S. F. (1986). *The Theory of Polymer Dynamics*. Vol. 73. International Series of Monographs on Physics. Oxford University Press.

Emmrich, E., Klapp, S. H. L., and Lasarzik, R. (2018). "Nonstationary models for liquid crystals: A fresh mathematical perspective". *Journal of Non-Newtonian Fluid Mechanics* **259**, 32–47. DOI: 10.1016/j.jnnfm.2018.05.003.

Evans, D. J., Hanley, H. J. M., and Hess, S. (1984). "Non-Newtonian phenomena in simple fluids". *Physics Today* **37**(1), 26. DOI: 10.1063/1.2916042.

Evans, D. J. and Morriss, G. (2008). *Statistical Mechanics of Nonequilibrium Liquids*. 2nd ed. Cambridge: Cambridge University Press. DOI: 10.1017/CBO9780511535307.

Filliger, R. and Reimann, P. (2007). "Brownian gyrator: a minimal heat engine on a nano scale". *Physical Review Letters* **99**, 230602. DOI: 10.1103/PhysRevLett.99.230602.

Foister, R. T. and van de Ven, T. G. M. (1980). "Diffusion of Brownian particles in shear flow". *Journal of Fluid Mechanics* **96**, 105–132. DOI: 10.1017/S0022112080002042.

Fokker, A. D. (1914). "Die mittlere Energie rotierender elektrischer Dipole im Strahlungsfeld". *Annalen der Physik* **43**(5), 810–820. DOI: 10.1002/andp.19143480507.

Forest, M. G., Wang, Q., and Zhou, R. (2004). "The flow-phase diagram of Doi-Hess theory for sheared nematic polymers II: finite shear rates". *Rheologica Acta* **44**, 80–93. DOI: 10.1007/s00397-004-0380-9.

Francaviglia, M., Restuccia, L., and Rogolino, P. (2004). "Entropy production in polarizable bodies with internal variables". *Journal of Non-Equilibrium Thermodynamics* **29**(3), 221–235. DOI: 10.1515/JNETDY.2004.052.

Franosch, T., Grimm, M., Belushkin, M., Mor, F. M., Foffi, G., Forró, L., and Jeney, S. (2011). "Resonances arising from hydrodynamic memory in brownian motion". *Nature* **478**, 85–88. DOI: 10.1038/nature10498.

Fuller, G. G. (1995). *Optical Rheometry of Complex Fluids*. Oxford University Press New York.

Gerloff, S., Ortiz-Ambriz, A., Tierno, P., and Klapp, S. H. L. (2020). "Dynamical modes of sheared confined microscale matter". *Soft Matter* **16**(41), 9423–9435. DOI: 10.1039/D0SM01238F.

Hess, S. and Rainwater, J. C. (1984). "Diffusion in a laminar flow: Shear rate dependence of correlation functions and of effective transport coefficients". *Journal of Chemical Physics* **80**(3), 1295–1303. DOI: 10.1063/1.446808.

Hess, S. (2015). *Tensors for Physics*. Heidelberg: Springer. DOI: 10.1007/978-3-319-12787-3.

Hess, S., Heidenreich, S., Ilg, P., Goddard, C., and Hess, O. (2008). "Thermodynamic and mesoscopic modelling of tumbling nematics, shear-thickening fluids and of stick-slip-like flow behavior". *Atti della Accademia Peloritana dei Pericolanti. Classe di Scienze Fisiche, Matematiche e Naturali* **86**, C1S0801010. DOI: 10.1478/C1S0801010.

Hess, S., Kröger, M., Loose, W., Pereira Borgmeyer, C., Schramek, R., H., V., and Weider, T. (1996). "Simple and complex fluids under shear". In: *Monte Carlo and Molecular Dynamics of Condensed Matter Systems*. Ed. by K. Binder and G. Ciccotti. Vol. 49. Conference Proceedings. Bologna, Italy: Società Italiana di Fisica.

Hess, S. (1976). "Fokker-Planck-Equation approach to flow alignment in liquid crystals". *Zeitschrift für Naturforschung A* **31**(9), 1034–1037. DOI: 10.1515/zna-1976-0902.

Holzer, L., Bammert, J., Rzehak, R., and Zimmermann, W. (2010). "Dynamics of a trapped Brownian particle in shear flows". *Physical Review E* **81** (4), 041124. DOI: 10.1103/PhysRevE.81.041124.

Hoover, W. G. (1986). *Molecular Dynamics*. Berlin, New York: Springer.

Janeschitz-Kriegl, H. (1983). *Polymer melt rheology and flow birefringence*. Berlin: Springer. DOI: 10.1007/978-3-642-68822-5.

Kirkwood, . G. (1946). "Statistical mechanical theory of transport processes I. General theory". *Journal of Chemical Physics* **14**, 180–201. DOI: 10.1063/1.1724117.

Kramers, H. A. (1940). "Brownian motion in a field of force and the diffusion model of chemical reactions". *Physica* **7**(4), 284–304. DOI: 10.1016/S0031-8914(40)90098-2.

Kröger, M. (2004). "Simple models for complex nonequilibrium fluids". *Physics Reports* **390**(6), 453–551. DOI: 10.1016/j.physrep.2003.10.014.

Kubo, R. (1966). "The fluctuation-dissipation theorem". *Reports on Progress in Physics* **29**(1), 255. DOI: 10.1088/0034-4885/29/1/306.

Langevin, P. (1908). "Sur la the théorie du mouvement brownien". *Comptes Rendus Hebdomadaires des Séances de l'Académie des Sciences* **146**(10), 530–533.

Larson, R. G. and Magda, J. J. (1989). "Coil-stretch transitions in mixed shear and extensional flow of dilute polymer solutions". *Macromolecules* **22**(7), 3004–3010. DOI: 10.1021/ma00197a022.

Loos, S. A. M. and Klapp, S. H. L. (2019). "Fokker-Planck equations for time-delayed systems via Markovian embedding". *Journal of Statistical Physics* **177**, 95–118. DOI: 10.1007/s10955-019-02359-4.

Loos, S. A. M. and Klapp, S. H. L. (2020). "Irreversibility, heat and information flows induced by non-reciprocal interactions". *New Journal of Physics* **22**, 123051. DOI: 10.1088/1367-2630/abcc1e.

Marteynec, T., Klapp, S. H. L., and Loos, S. A. M. (2020). "Entropy production at criticality in a nonequilibrium Potts model," *New Journal of Physics* **22**, 093069. DOI: 10.1088/1367-2630/abb5f0.

Maugin, G. A. and Muschik, W. (1994). "Thermodynamics with internal variables. Part I. General concepts". *Journal of Non-Equilibrium Thermodynamics* **19**(3), 217–249. DOI: 10.1515/jnet.1994.19.3.217.

Maxwell, J. C. (1874). "IV. On double refraction in a viscous fluid in motion". *Proceedings of the Royal Society of London* **22** (148–155), 46–47. DOI: 10.1098/rspl.1873.0011.

Mitterwallner, B. G., Schreiber, C., Daldrop, J. O., Rädler, J. O., and Netz, R. R. (2020). "Non-markovian data-driven modeling of single-cell motility". *Physical Review E* **101**(3), 032408. DOI: 10.1103/PhysRevE.101.032408.

Netz, R. R. (2020). "Approach to equilibrium and nonequilibrium stationary distributions of interacting many-particle systems that are coupled to different heat baths". *Physical Review E* **101**(2), 022120. DOI: 10.1103/PhysRevE.101.022120.

Peterlin, A. and Stuart, H. A. (1943). "Doppelbrechung: insbesondere künstliche Doppelbrechung". In: *Handbuch und Jahrbuch der chemischen Physik Band 8, Abschnitt 1B*. Ed. by A. Eucken and K. L. Wolf. Vol. 8. Leipzig, Deutschland: Akademische Verlagsgesellschaft.

Planck, M. (1917). *Über einen Satz der statistischen Dynamik und eine Erweiterung der Quantentheorie*. Sitzungsberichte der Königlich Preussischen Akademie der Wissenschaften zu Berlin. Berlin: Reimer, pp. 324–341.

Restuccia, L. and Kluitenberg, G. A. (1988). "On generalizations of the Debye equation for dielectric relaxation". *Physica A* **154**(1), 157–182. DOI: 10.1016/0378-4371(88)90186-0.

Restuccia, L. and Kluitenberg, G. A. (1990). "Hidden vectorial variables as splitting operators for the polarization vector in the thermodynamic theory of dielectric relaxation". *Journal of Non-Equilibrium Thermodynamics* **15**, 335. DOI: 10.1515/jnet.1990.15.4.335.

Risken, H. (1984). *The Fokker-Planck Equation. Methods of Solution and Applications*. Berlin: Springer. DOI: 10.1007/978-3-642-96807-5.

Seifert, U. (2005). "Entropy production along a stochastic trajectory and an integral fluctuation theorem". *Physical Review Letters* **95**(4), 040602. DOI: 10.1103/PhysRevLett.95.040602.

Seifert, U. (2012). "Stochastic thermodynamics, fluctuation theorems and molecular machines". *Reports on Progress in Physics* **75**(12), 126001. DOI: 10.1088/0034-4885/75/12/126001.

Siegle, P., Goychuk, I., Talkner, P., and Hänggi, P. (2010). "Markovian embedding of non-Markovian superdiffusion". *Physical Review E* **81**(1), 011136. DOI: 10.1103/PhysRevE.81.011136.

Smoluchowski, M. V. (1916). "Über Brownsche Molekularbewegung unter Einwirkung äußerer Kräfte und deren Zusammenhang mit der verallgemeinerten Diffusionsgleichung". *Annalen der Physik* **353**(24), 1103–1112. DOI: 10.1002/andp.19163532408.

Verlet, L. (1967). "Computer "experiments" on classical fluids I. Thermodynamical properties of Lennard-Jones molecules". *Physical Review* **159**(1), 98. DOI: 10.1103/PhysRev.159.98.

Vezirov, T. A. and Klapp, S. H. L. (2013). "Nonequilibrium dynamics of a confined colloidal bilayer in a planar shear flow". *Physical Review E* **88**(5), 052307. DOI: 10.1103/PhysRevE.88.052307.

[a] Technische Universität Berlin,
Sekr. EW 7-1, Institut für Theoretische Physik,
Hardenbergstr. 36, D-10623 Berlin, Germany

* To whom correspondence should be addressed | email: s.hess@campus.tu-berlin.de

Communicated 24 May 2022; manuscript received 28 July 2022; published online 17 February 2023